Design Principles of a Conditional Futile Cycle Exploited for Regulation

Dean A. Tolla[a], Patricia J. Kiley[c], Jason G. Lomnitz[a], and Michael A. Savageau[a,b*]

[a]*Biomedical Engineering Department and* [b]*Microbiology Graduate Group, University of California, One Shields Ave, Davis, CA 95616 USA.*

[c]*Department of Biomolecular Chemistry, University of Wisconsin, 1300 University Avenue, Madison, WI 53706*

*Corresponding Author: masavageau@ucdavis.edu, Tel. +1 530 754 7350, Fax +1 530 754 5739

SUPPLEMENTARY INFORMATION

Deconstructing Transitions Between Aerobic And Anaerobic States.

The transitions between aerobic and anaerobic environments (**Fig. 3** in the main text) have two key temporal behaviors: a short-term peak, followed by a long-term relaxation to a stable state. These two behaviors arise from the difference in time-scale between rapid cycling of the FNR regulator, and slow dilution of regulatory protein by growth and genetic regulation of the *fnr* gene. Here, we show the contributions of these processes by deconstructing the model into the fast and slow sub-systems, as shown in **Fig. S1**. The essential features of these sub-systems can be illustrated with simplified models in which the mRNA pool is in quasi-steady state and

represented implicitly, repression is treated as a conventional Hill function, and all the remaining reactions are treated as first order.

Aerobic to anaerobic transition

The aerobic steady state (Fig. S1A) is governed by the follow equations

$$\frac{dX_2}{dt} = \gamma - \delta_2 X_2 \qquad \frac{dX_3}{dt} = \alpha X_2^2 - \beta X_3 \tag{S1}$$

$$X_{20} = \gamma / \delta_2 \qquad X_{30} = \alpha(\gamma / \delta_2)^2 / \beta \qquad 0.5X_{20} + X_{30} = T_A \tag{S2}$$

where γ is the maximum rate of synthesis of X_2, δ_2 is the rate constant for loss of X_2, α is the rate constant for the dimerization of inactive FNR (X_2), β is the rate constant for the inactivation of active FNR (X_3), the steady-state values of X_2 and X_3 are given with the additional "o" subscript, and T_A is the sum of the material in the aerobic cycle in units of X_3.

In the fast phase of the transition to the anaerobic state (Fig. S1B), the cycle is abruptly interrupted. The steady-state solutions, Eqs. (S2), are the initial conditions for the simplified equations governing the fast dynamics:

$$\frac{dX_2}{dt} = -2\alpha X_2^2 \qquad \frac{dX_3}{dt} = 4\alpha(T_A - X_3)^2 \tag{S3}$$

$$X_{20} = 0 \qquad X_{30} = T_A \tag{S4}$$

In the slow phase of the transition to the anaerobic state (Fig. S1C), the steady-state solutions, Eqs. (S4), become the initial conditions. The simplified equations governing the slow dynamics, which involve repression of the *fnr* gene and dilution of X_3 are the following:

$$\frac{dX_2}{dt} = \gamma \frac{K_H}{K_H + X_3} - 2\alpha X_2^2 \qquad \frac{dX_3}{dt} = \alpha X_2^2 - \delta_3 X_3 \tag{S5}$$

$$X_{30} = \frac{1}{2}\left\{\sqrt{K_H^2 + \frac{2\gamma K_H}{\delta_3}} - K_H\right\} \qquad X_{20} = \sqrt{(\delta_3/\alpha)X_{30}} \qquad 0.5X_{20} + X_{30} = T_N \tag{S6}$$

where K_H is concentration of X_3 for half-maximal repression, δ_3 is the first-order rate constant for the loss of active FNR and T_N is the sum of the material in the anaerobic cycle in units of X_3.

Anaerobic to aerobic transition

The anaerobic steady state (Fig. S1D) is governed by Eqns. (S5) and (S6). In the fast phase of the transition to the aerobic state (Fig. S1E), the cycle is abruptly reestablished. The steady-state solutions, Eqs. (S6), become the initial conditions for the simplified equations governing the fast dynamics:

$$\frac{dX_2}{dt} = 2\beta X_3 - 2\alpha X_2^2 \qquad \frac{dX_3}{dt} = \alpha X_2^2 - \beta X_3 \tag{S7}$$

$$X_{20} = \frac{\beta}{4\alpha}\left\{\sqrt{1 + \frac{16\alpha}{\beta}T_N} - 1\right\} \qquad X_{30} = T_N - 0.5X_{20} \tag{S8}$$

In the slow phase of the transition to the aerobic state (Fig. S1F), the steady-state solutions, Eqs. (S8), become the initial conditions. The simplified equations governing the slow dynamics are again Eqns. (S1) and (S2), which involve derepression of the *fnr* gene and dilution of X_2.

The temporal behavior of the fast and slow components of each transition is shown independently in **Fig. S2**. This deconstruction provides insight into the role of rapid cycling and genetic regulation to the characteristic response of systems with conditional futile cycles. The anaerobic-to-aerobic transition involves (1) restoration of the FNR cycle (**Fig. S1A**) and a shift to the inactive form of FNR (**Fig. S2A)**, followed by (2) de-repression of *fnr* expression (**Fig S1B**) resulting in a relaxation to the aerobic levels of active and inactive FNR (**Fig. S2B**). Similarly, the aerobic-to-anaerobic transition involves (1) interruption of the FNR cycle (**Fig. S1C**) and an almost complete shift from inactive to active FNR (**Fig. S2C**), followed by (2) repression of *fnr* expression by active FNR (**Fig S1D**) resulting in a relaxation to the anaerobic levels of active and inactive FNR (**Fig. S2D**).

Increasing *fnr* Copy Number is Not Predicted to Alter the Cycling Mechanism

In a further effort to manipulate the cycling rate, we have assessed the effects of increasing the *fnr* gene dose in the model, and our analysis reveals that attempts to influence cycling rate by this method have a negligible effect on the observable behavior of the system. After making an adjustment to the transcription rate constant ($\alpha_{1,\max}$) that reflects the increased gene-copy number, we can predict the resulting behavior of the system, and assess the ability of the gene dosage to influence specific attributes of the model. Experimental measurement of total

FNR concentration has been examined for cells containing one, two, or three copies of the *fnr* gene (see[17] in main text). We can adjust the transcription rate constant ($\alpha_{1,\max}$) such that the total FNR concentration in the model agrees with the experimental characterization of the relationship between *fnr* copy number and total FNR levels (see **Materials and Methods** in main text).

Increased transcription results in three simultaneous changes to the FNR system, by changing the throughput flux, steady-state concentration, and cycling rate (**Fig. S3**). First, more material coming into the system results in more material flowing out of the system at steady state and consequently total throughput is increased. Second, the steady-state concentrations of active FNR and inactive FNR increase, and third, the changes in steady state increase the rate of material cycling within the system. The ability to decouple these co-occurring effects (cases A, B, and C in **Fig. S3**) and assess their individual and paired contributions is one advantage of our mathematical approach. We accomplish the goal of untangling each effect from the complete copy-number variant by introducing constraints. For example, to single out the throughput effect, total throughput is constrained to match its value in the copy-number variant while the steady-state and cycling effects are constrained to match their values in the wild-type. Each effect is looked at individually and then all possible pairs of effects are examined. Combining all three effects together represents the copy-number variant observed experimentally in the laboratory. The precise throughput, steady state, and cycling values used in each of the cases and the details of the parameter changes used to constrain the model are provided in the **Materials and Methods** section of the main text.

The predicted aerobic-to-anaerobic dynamic response of the FNR circuit carrying four copies of the *fnr* gene is compared with the wild-type in **Fig. S4**. The magnitude of the overshoot in the variant is almost double that of the wild-type; the predicted overshoot in the dynamic

reporter assay also doubles and peaks at 135% of its anaerobic steady-state activity (**Fig. S5**). The analysis of the individual contributions from changes in throughput, steady state, and cycling (**Fig. S4** panels **A**, **B**, and **C**) indicate that the qualitative shape of the dynamics in the copy-number variant are dominated by the throughput effect. This effect alone is sufficient to reproduce the shape of the dynamics including the overshoot, but differs from the copy-number variant on three quantitative aspects; the magnitude of the overshoot is too large, the peak time is too fast, and the settling time is too fast. Combining the throughput and steady-state effects results in dynamics that match the magnitude of the overshoot and the settling time of copy-number variant (**Fig. S4E**). The peak time that results when pairing these two effects still deviates slightly from the variant. Our analysis indicates that the altered dynamics of the FNR circuit that result from increasing the number of *fnr* gene copies depends far more upon changing the throughput and steady state of the system than it does the cycling (**Fig. S4**) with throughput being the dominant influence.

Framework for Copy-Number Variant Analysis

The relationship between *fnr* gene copy number and steady-state FNR levels involves changes in the rate constant for transcription, which can be derived from experimental data measured by Mettert and Kiley (see[17] in main text). The presence of a plasmid containing 1, 2, or 3 copies of the *fnr* gene in an *fnr*$^-$ background resulted in cells containing 23.3 ± 0.9, 33.5 ± 1.5, and 45.1 ± 2.1 pg of FNR/μL of cells when grown to an OD_{600} of 0.2, respectively. Under the same conditions, wild-type cells contained 68 ± 0.8 pg of FNR protein/μL of cells. Thus, cells carrying only one plasmid copy of the *fnr* gene contained ~ 33 % of the wild-type FNR

concentration. This fixes the transcription rate constant of plasmid derived FNR from a single gene copy at 0.33 of the rate constant for the chromosomal gene ($\alpha_{1,\max}$). For the plasmid gene copies, the expression ratios for 2:1, 3:2, and 3:1 copies were 1.44 ± 0.08, 1.35 ± 0.09, and 1.94 ± 0.12, respectively. The relationship between total FNR, as predicted by the model, and the FNR expression ratios, as determined experimentally, involves changes in the rate constant for transcription that is accurately fit by the relationship $(0.17 + 0.158n)\alpha_{1,\max}$, with a root-mean-square error of 0.047. Since we wish to overexpress FNR in order to examine the feasibility of capturing the predicted overshoot experimentally, including the chromosomal copy of *fnr* works to our benefit. Thus, the final relationship for change in the rate constant for transcription used in the simulations for this study is

$$\alpha'_{1,\max} = \alpha_{1,\max}(1.17 + 0.158n) \tag{S14}$$

To formulate the constraints used in analyzing the copy-number variant in the text, we begin by solving numerically for the steady-state values of the copy-number variant and denote them as X'_{10}, X'_{20}, X'_{30}. Note that when we need to constrain the steady-state values of the copy-number variant to their wild-type values, we can only require $X'_{20} = X_{20}$ and $X'_{30} = X_{30}$. The additional requirement that $X'_{10} = X_{10}$ could only be achieved by altering the decay of the message ($\beta_{1,\max}/\beta_{1,\min}$) in coordination with the increased transcription rate, but this would negate the effects of increasing the copy-number before its influence propagates through the system.

The constraints used to examine the individual and paired effects of throughput, cycling, and steady state are specific for each case, but all are based on the following equations in which the constrained quantities have a double prime. The rate constants for disassociation and decay

of dimeric FNR (α''_{22} , $\beta''_{31,\min}$, $\beta''_{31,\max}$) will also be specified in each case. The steady-state values of the wild type are unprimed and those of the case-by-case alternatives, when they differ from the wild type, are double-primed (X''_{10} , X''_{20} , X''_{30}). The double-prime variables X''_{20} and X''_{30} are simply placeholders, and their values will be specified in each case. Equation (S15) shows how each case affects the steady state of X_1 and the other case-specific parameters. Recall that primed values (X'_{10}, X'_{20}, X'_{30}) refer to the unconstrained steady-state solution of the copy-number variant.

$$X''_{10} = \frac{\alpha'_{1,\max} K_1 \left(K_2^n + X_{6,\max}^n \right)}{\left(X''_{30} + K_1 \right) \left(\beta_{1,\min} K_2^n + \beta_{1,\max} X_{6,\max}^n \right)} \tag{S15}$$

$$\beta''_{22} = \frac{X''_{30} \left(\alpha''_{22} X_{6,\max} \left[K_2^n + X_{6,\max}^n \right] + \beta''_{31,\min} K_2^n + \beta''_{31,\max} X_{6,\max}^n \right)}{\left(X''^2_{20} X_5 \left[K_2^n + X_{6,\max}^n \right] \right)} \tag{S16}$$

$$\beta''_{21,\min} = \frac{\beta_{21,\min} \left(\alpha_{21} X''_{10} + 2\alpha''_{22} X''_{30} X_{6,\max} - 2\beta''_{22} X''^2_{20} X_5 \right) \left(K_2^n + X_{6,\max}^n \right)}{X''_{20} X_4 \left(\beta_{21,\min} K_2^n + \beta_{21,\max} X_{6,\max}^n \right)} \tag{S17}$$

$$\beta''_{21,\max} = \beta_{21,\max} \beta''_{21,\min} / \beta_{21,\min} \tag{S18}$$

We show how increasing the *fnr* gene copy number influences the dynamic and steady-state characteristics of the system by assessing three factors, separately and in combination, that contribute to the phenotype of a copy-number variant: flux of protein through the system (changes in throughput), flux of protein moving through the cycle (changes in cycling), and the steady-state concentrations of *fnr* mRNA and protein (changes in steady state).

Case 1: Throughput matches the copy-number variant. Cycling and steady state are constrained to their wild-type values. Constraining the steady state to the wild-type implies $X''_{20} = X_{20}$ and $X''_{30} = X_{30}$. Cycling remains unchanged provided $\alpha''_{22} = \alpha_{22}$, since the steady state is unchanged and the cycling rate is given by $\alpha''_{22} X_{30} X_{6,\max}$. The copy-number variant throughput is given by $(\beta_{31,\min} K_2^n + \beta_{31,\max} X_{60}^n) X'_{30} \big/ (X_{60}^n + K_2^n)$, and since we have fixed $X''_{30} = X_{30}$ in our control model, we must alter $\beta_{31,min}/\beta_{31,max}$ in order to match the variant throughput. The appropriate rate constants for decay of the FNR dimer are given by $\beta''_{31,\min} = \beta_{31,\min} X'_{30} / X_{30}$ and $\beta''_{31,\max} = \beta_{31,\max} X'_{30} / X_{30}$.

Case 2: Cycling matches the copy-number variant. Throughput and steady state are constrained to the wild-type values. As in the previous case, matching the steady state to the wild-type implies $X''_{20} = X_{20}$ and $X''_{30} = X_{30}$. Throughput remains unchanged provided $\beta''_{31,\max} = \beta_{31,\max}$ and $\beta''_{31,\min} = \beta_{31,\min}$. The copy-number variant cycling rate is given by $\alpha_{22} X'_{30} X_{6,\max}$, and since we have fixed $X''_{30} = X_{30}$, we must alter α_{22} in order to match the cycling rate of the variant. The appropriate rate constant for disassociation of the FNR dimer is given by $\alpha''_{22} = \alpha_{22} X'_{30} / X_{30}$.

Case 3: Steady state matches the copy-number variant. Throughput and cycling are constrained to the wild-type values. In this case, matching the steady state to the copy-number variant implies $X''_{20} = X'_{20}$ and $X''_{30} = X'_{30}$. The steady state of the variant will also change the rate of throughput and the cycling rate; we must change α_{22} and $\beta_{31,min}/\beta_{31,max}$ in order to match the wild-type. The appropriate rate constants for decay of the FNR dimer are given by $\beta''_{31,\min} = \beta_{31,\min} X_{30} / X'_{30}$ and $\beta''_{31,\max} = \beta_{31,\max} X_{30} / X'_{30}$, and the appropriate rate constant for disassociation of the FNR dimer is given by $\alpha''_{22} = \alpha_{22} X_{30} / X'_{30}$.

Case 4: Throughput and cycling match the copy-number variant. The steady state is constrained to the wild-type value. Constraining the steady state to the wild-type implies $X''_{20} = X_{20}$ and $X''_{30} = X_{30}$. The rate of throughput for the copy-number variant is matched as in Case 1, and the cycling rate is matched as in Case 2. Thus, the appropriate rate constants for decay of the FNR dimer are given by $\beta''_{31,\min} = \beta_{31,\min} X'_{30} / X_{30}$ and $\beta''_{31,\max} = \beta_{31,\max} X'_{30} / X_{30}$, and the appropriate rate constant for disassociation of the FNR dimer is given by $\alpha''_{22} = \alpha_{22} X'_{30} / X_{30}$.

Case 5: Throughput and steady state match the copy-number variant. Cycling is constrained to the wild-type value. Constraining the steady state to the copy-number variant implies $X''_{20} = X'_{20}$ and $X''_{30} = X'_{30}$. Because the steady state values of the variant are used, the rate of throughput will match the copy-number variant provided $\beta''_{31,\min} = \beta_{31,\min}$ and $\beta''_{31,\max} = \beta_{31,\max}$. The cycling rate must be constrained to the wild-type as in Case 3, which implies that the appropriate rate constant for disassociation of the FNR dimer is given by $\alpha''_{22} = \alpha_{22} X_{30} / X'_{30}$.

Case 6: Cycling and steady state match the copy-number variant. Throughput is constrained to the wild-type value. Constraining the steady state to the copy-number variant implies $X''_{20} = X'_{20}$ and $X''_{30} = X'_{30}$. Because the steady state values of the variant are used, the cycling rate will match the copy-number variant provided $\alpha''_{22} = \alpha_{22}$. The rate of throughput must be constrained to the wild-type as in Case 3, which implies that the appropriate constants for decay of the FNR dimer are given by $\beta''_{31,\min} = \beta_{31,\min} X_{30} / X'_{30}$ and $\beta''_{31,\max} = \beta_{31,\max} X_{30} / X'_{30}$.

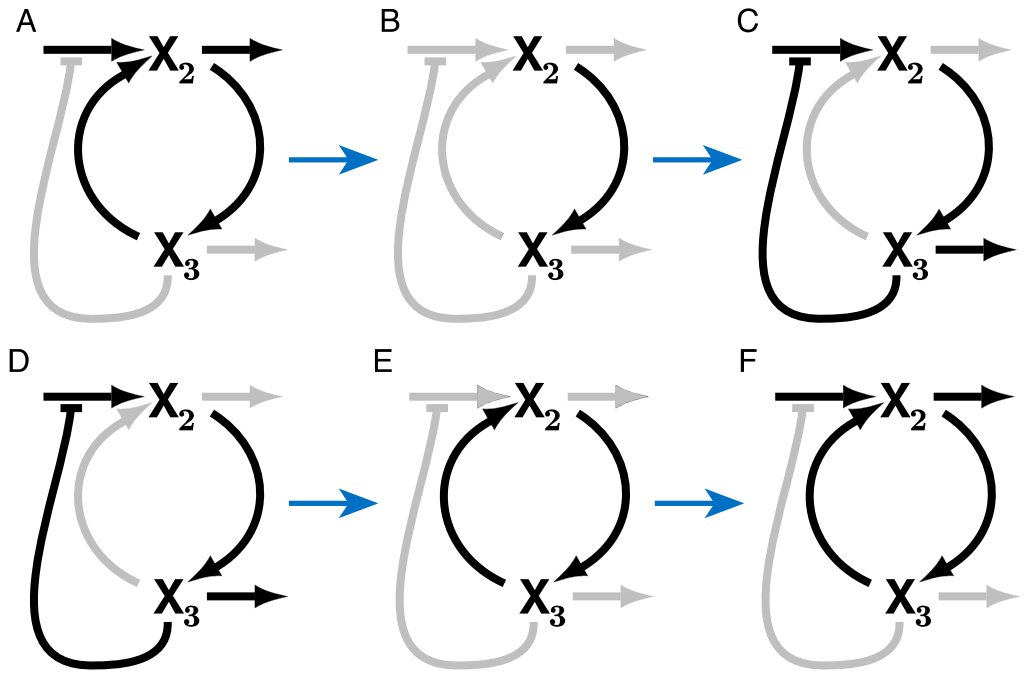

Figure S1: Deconstruction of the general FNR model into sub-systems governing the fast and slow temporal responses. The fast response from aerobic to anaerobic conditions starts from the aerobic steady (A) and switches with an abrupt interruption of the cycle (B) and then progresses slowly to the anaerobic steady state (C). The fast response from anaerobic to aerobic conditions starts from the anaerobic steady state (D) and switches with an abrupt reestablishment of the cycle (E) and then progresses slowly to the aerobic steady state (F).

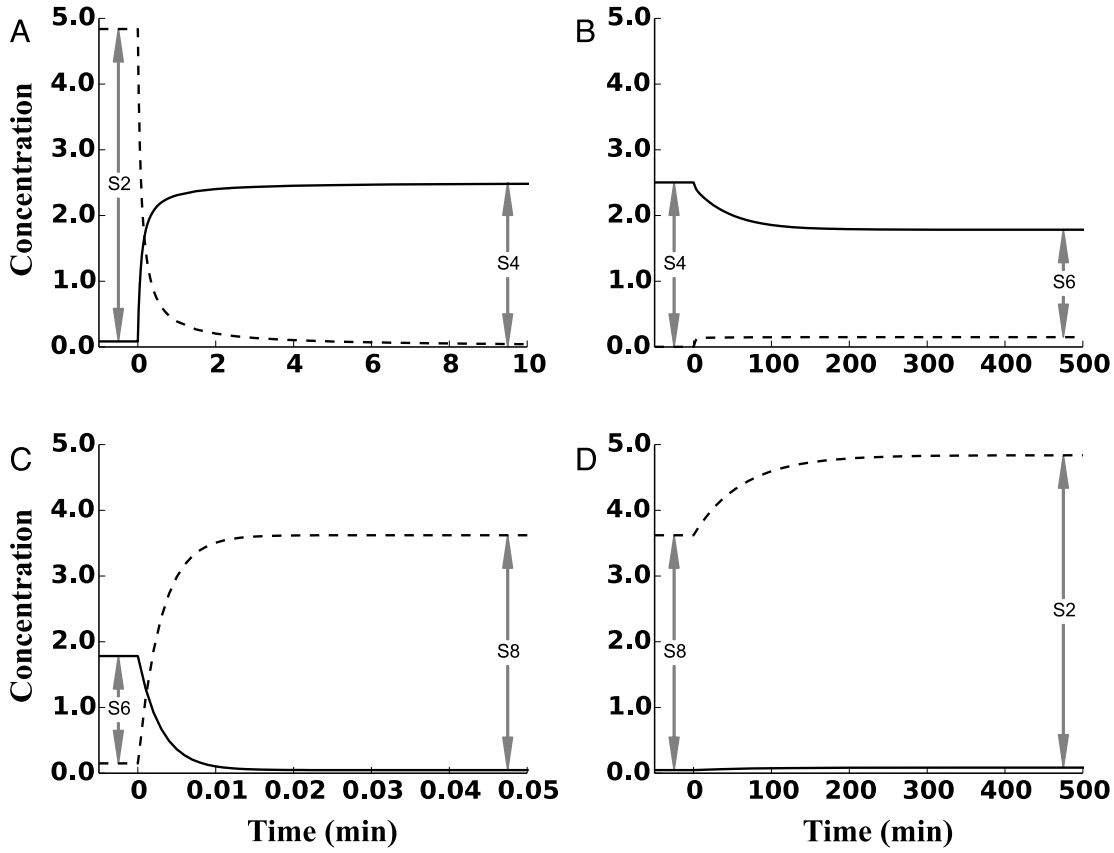

Figure S2. Temporal responses during transitions between anaerobic and aerobic conditions. (A)-(B) Transition form aerobic to anaerobic conditions. (C)-(D) Transition form anaerobic to aerobic conditions. (A,C) Fast initial response; (B, D) Slow long-term response. Solid lines represent active FNR; dashed lines represent inactive FNR. Labels in between steady-state values (at the beginning and end of the simulations) indicate the supplemental equations [S2, S4, S6 or S8]. The parameter values used for the simulation are: $\alpha = 1.183$, $\beta = 327.2$, $K_H = 1.75$, $T_A = 2.5$ and $T_N = 1.859$. For the aerobic to anaerobic transition, $\gamma = 0.0779$ $\delta_2 = 0.0161$, $\delta_3 = 0.0231$. For the anaerobic to aerobic transition, $\gamma = 0.1066$, $\delta_2 = 0.0124$, $\delta_3 = 0.0148$.

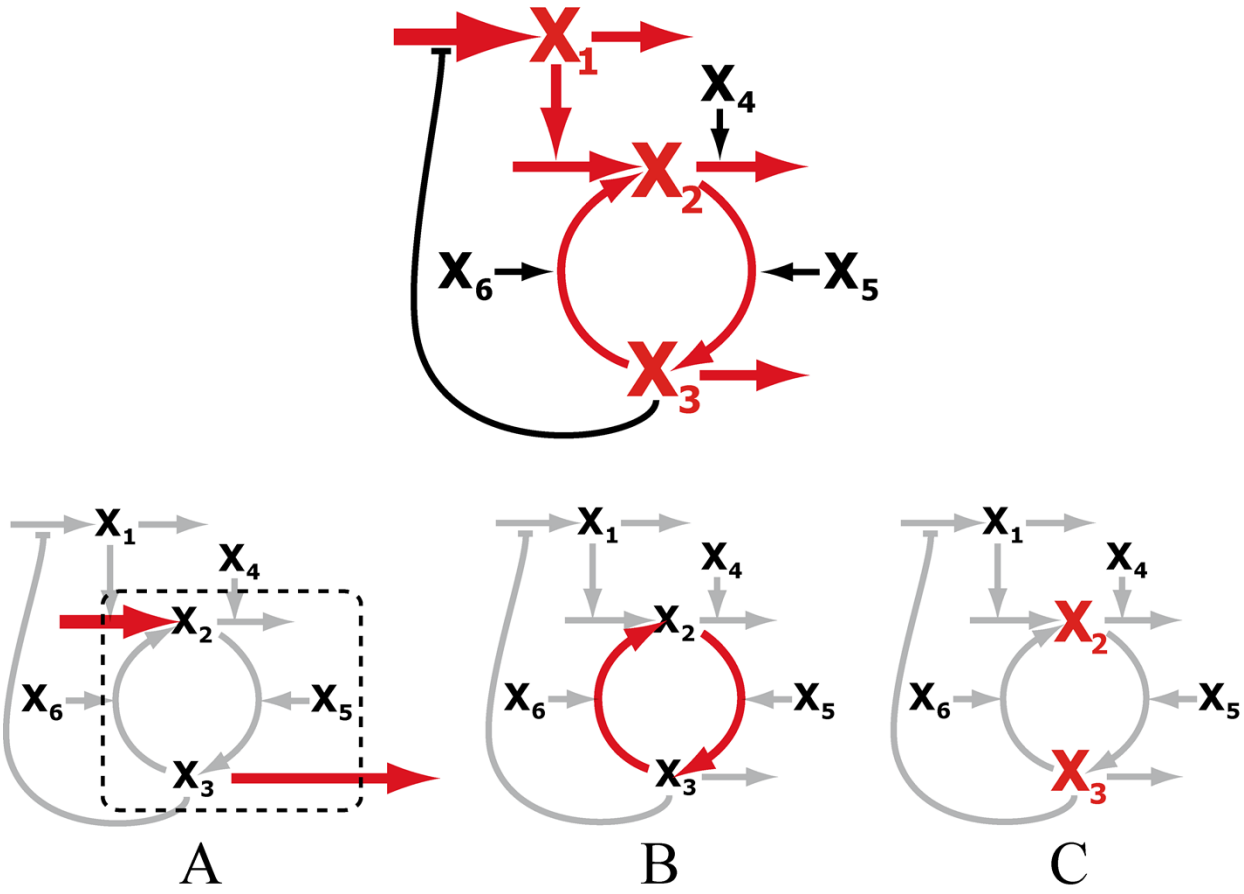

Figure S3. Composite Effects of Increased *fnr* Gene Copy Number

Increasing the number of *fnr* gene copies alters the (A) throughput, (B) cycling, and (C) steady states of the FNR regulatory network. Red arrows indicate processes that are altered and gray arrows indicate processes that are mathematically constrained to the wild-type behavior.

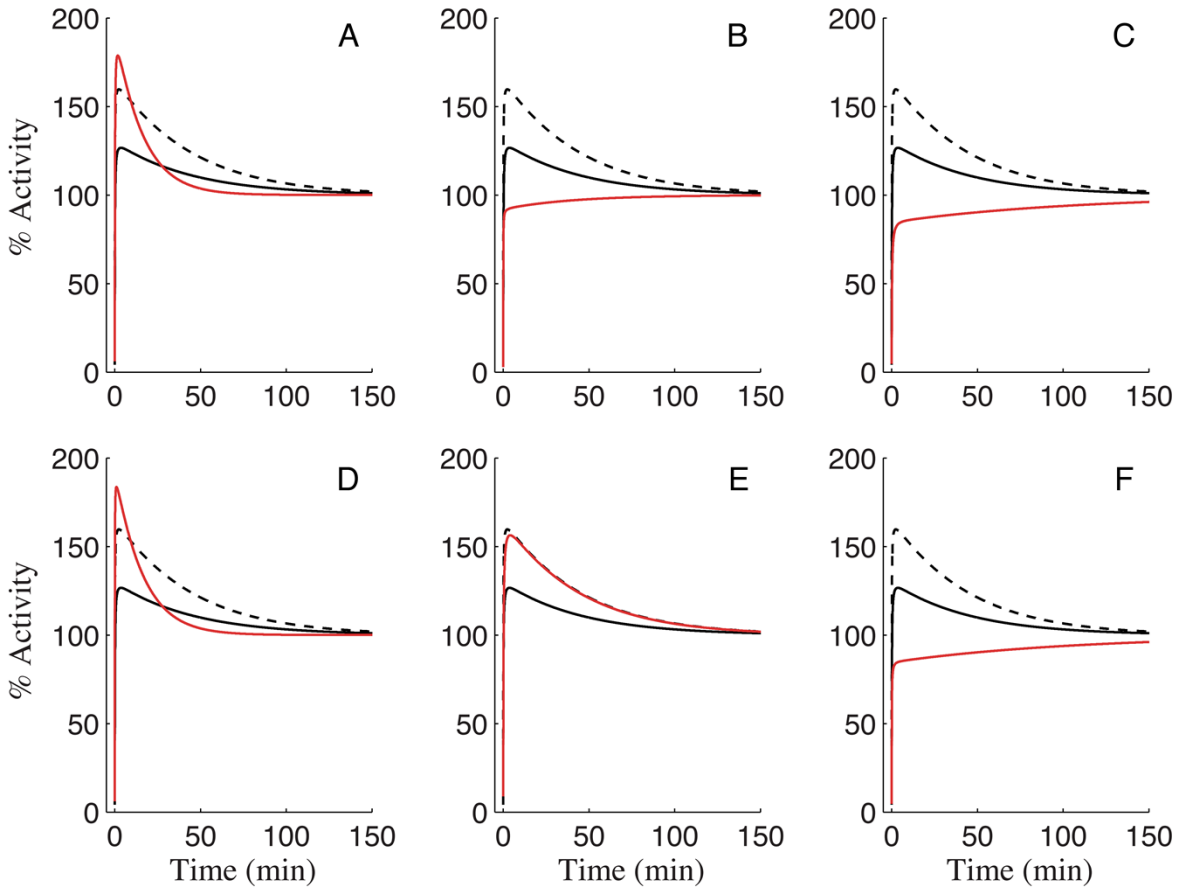

Figure S4. Assessing the Component Effects on the Phenotype of Copy-Number Variants

Predicted dynamics of the aerobic-to-anaerobic transition for the wild-type (—) and variant strain carrying 4 copies of the *fnr* gene (– –). The red curve in each panel shows the predicted dynamics attributable to individual or paired effects: (A) throughput, (B) cycling, (C) steady state, (D) throughput and cycling, (E) throughput and steady state, and (F) cycling and steady state. Note that the paired effects in case E closely match the dynamics of the variant strain (– –), and that the variant strain corresponds to the combination of all three effects: throughput, cycling and steady state.

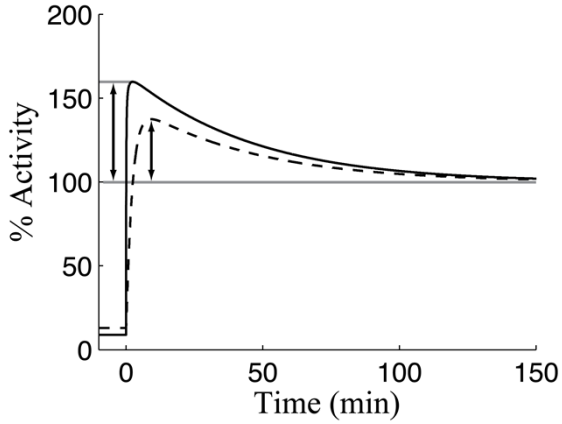

Figure S5. Exaggerating the Overshoot in Active FNR Dynamics

Predicted dynamics for the accumulation of active FNR in a copy-number variant carrying 4 copies of the *fnr* gene (—) and its value inferred from the simulated *dms*A-*lac*Z reporter (– –). The double arrows indicate the magnitude of the overshoot, which is 60% for the overexpressed active FNR and 35% for the *dms*A-*lac*Z reporter.